ACS APPLIED MATERIALS & INTERFACES

Research Article

www.acsami.org

Growth of Solid and Hollow Gold Particles through the Thermal Annealing of Nanoscale Patterned Thin Films

Junhao Lin,[†,‡,#] Weidong He,[‡,§,∥,#] Subramanian Vilayurganapathy,[⊥,⊗] Samuel J. Peppernick,[∥] Bin Wang,[†] Sandeep Palepu,[†] Miroslav Remec,[†] Wayne P. Hess,[∥] Anthony B. Hmelo,[†,‡] Sokrates T. Pantelides,[†,‡] and James H. Dickerson*[,†,‡]

[†]Department of Physics and Astronomy, Vanderbilt University, Nashville, Tennessee 37235-1807, United States

[‡]Vanderbilt Institute of Nanoscale Science and Engineering and [§]Interdisciplinary Program in Materials Science, Vanderbilt University, Nashville, Tennessee 37235-0106, United States

[∥]Chemical and Materials Science Division and [⊥]Environmental Molecular Sciences Laboratory, Pacific Northwest National Laboratory, P.O. Box 999, Richland, Washington 99352, United States

[⊗]Western Michigan University, 1903 West Michigan Ave, Kalamazoo, Michigan 49008, United States

Supporting Information

ABSTRACT: Through thermally annealing well-arrayed, circular, nanoscale thin films of gold, deposited onto [111] silicon/silicon dioxide substrates, both solid and hollow gold particles of different morphologies with controllable sizes were obtained. The circular thin films formed individual particles or clusters of particles by tuning their diameter. Hollow gold particles were characterized by their diameter, typically larger than 400 nm; these dimensions and properties were confirmed by cross-section scanning electron microscopy. Hollow gold particles also exhibited plasmonic field enhancement under photoemission electron microscopy. Potential growth mechanisms for these structures were explored.

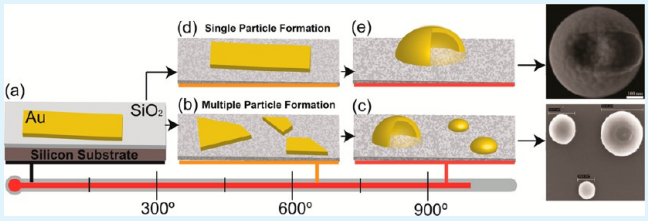

KEYWORDS: *hollow gold particle, thermal annealing, e-beam lithographical patterning, focused ion beam, photoemission electron microscopy*

I. INTRODUCTION

Gold crystalline structures have been the subject of considerable research interest because of their size-dependent optical properties, such as surface plasmon resonance and surface enhanced Raman scattering.[1−7] Patterning individual gold nanostructures into an ordered array is an effective way to increase the intercoupling between the nanostructures, which leads to a further enhancement of the aforementioned size-dependent properties for plasmonic and sensing applications.[8,9] Among the variety of possible approaches toward patterning of gold nanostructures, well-arrayed assembling of hollow gold particles, which are of particular interest because of the shell-induced local trapping of surface plasmon,[4−6] have not been possible using conventional top-down fabrication techniques because of the difficulties in constructing the inner cavity inside of the three-dimensional particle.

Recent research has demonstrated that solid gold particles of various shapes and sizes could be produced from uniform deposited gold films that are subjected to thermal annealing. Specifically, arrays of solid gold particles were realized by annealing patterned gold films, fabricated by nanosphere lithography.[10−12] Although the reported results suggest that thermal annealing can serve as an effective post-treatment to engineer the gold nanostructures from a flat two-dimension-like thin film to three-dimensional structures, the size of as-formed particles is not controllable and tunable. Moreover, these particles are found to be solid, which lowers their response to optical plasmonic signals and limits their real-world applications.

In this article, we reported a controllable top-down fabrication procedure for well-ordered, solid and hollow gold particle arrays with tunable properties, fabricated by a combination of electron beam lithography (with control over the diameters of individual films) and thermal annealing of metallic thin films. Further, the synthesized hollow gold structures were characterized by observing their cross sections, prepared by focus ion beam sectioning (FIB). The optical response and near field enhancement of the synthesized gold particles were studied using photoemission electron microscopy (PEEM). Finally, the formation mechanisms of hollow and solid gold particles were explored. Our studies reveal a promising method to produce hollow gold particles of tunable diameter with near field optical enhancement characteristics, all of which may lead to myriad potential applications in plasmonics.

Received: July 3, 2013
Accepted: October 21, 2013
Published: October 21, 2013

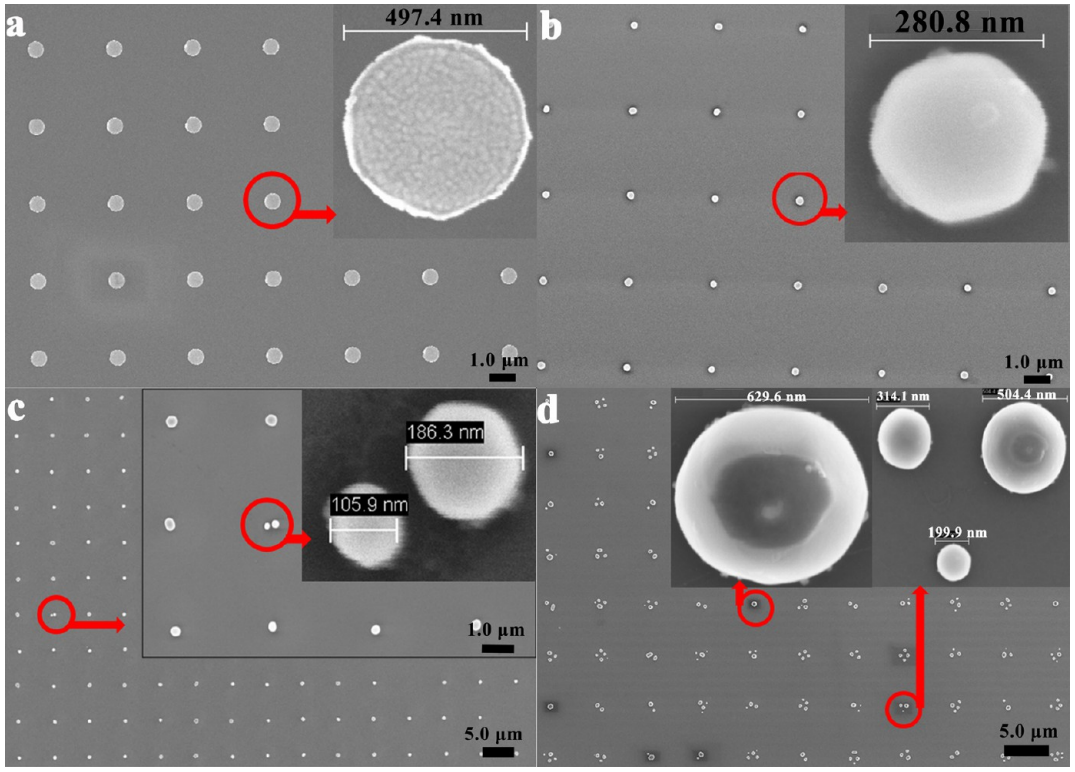

Figure 1. SEM images, illustrating different paths toward the formation of single and multiple gold particles as a function of patterned film diameter. Each array contained 50 × 50 individual films. (a) Circular films of diameter 500 nm prior to annealing. (b) Gold particles of diameter ∼280 nm, formed through annealing gold films in panel a at 940 °C for 10 h. (c) Gold particles formed from 900 nm films. This diameter of the gold films marked the onset diameter for the formation of multiple particles. Inset: Magnified image of the multiple gold particles. (d) Gold particles that formed from films that were 2000 nm in diameter. Two types of formations (Large single hollow particles and small multiple solid particle arrays) were observed, as shown in the inset.

EXPERIMENTAL SECTION

Preparation of Gold Particles from Patterned Nanoscale Gold Film via Annealing. Arrays of gold particles with diameters from 100 to 2000 nm were produced by electron beam lithography using the following algorithm: a 50 nm layer of PMMA electron beam resist was spin-coated onto a [111] silicon substrate (Sumitomo Sitix Silicon) with an extant native oxide layer. Predesigned patterns were written on the sample by electron beam lithography (EBL, Raith eLiNE operating in writing mode); the resist-covered substrate was then developed in MIBK:IPA (1:3) for 45 s; next, 20 nm of gold was deposited by e-beam evaporation (Åmod 600, Angstrom Engineering Inc.); after lifting off the unwanted PMMA, the desired gold patterned film remained. A scanning electron microscopy (SEM, Raith eLiNE at 20 kV) image in Figure 1a illustrates circular gold patterned films that are 500 ± 15 nm in diameter and 20 ± 2 nm in thickness. The gold grains within the as-deposited films were observed to be several tens of nm in size, indicating they are wholly polycrystalline. The well-arrayed gold particles, as shown in Figure 1b, were attained after inserting the gold films into a quartz tube in a horizontal tube furnace (Thermolyne #F21135 furnace, Barnstead International) for a time-sensitive reformation step under a stream of dry, ultrapure nitrogen (100 sccm) for 10 h at 940 ± 5 °C. The gold film thickness, annealing time, annealing temperature, and nitrogen flow rate were set the same for all of the experiments.

Statistical Counting of the Percent of Multiple Formation in One Film Size. Arrays containing 50 × 50 patterned gold films (totaling 2500 individual patterned gold films) were fabricated for the experiments; each circular patterned film possessed a different diameter in a range from 100 to 2000 nm (100 nm as a step). After annealing, the gold particles formed, and the sample was sent to SEM for assessment. For each film diameter, we performed a statistical analysis of the behavior and evolution of said film as a function of the film's initial diameter. For example, we counted the total number of films of a specified diameter that eventually yielded multiple nanoscale and/or microscale particles. After examining the entire 50 × 50 array, we divided the total number of occurrences of multiple particle formation by the total number of the films in an array (for all diameters), which yielded the percent of multiple particle formation as a function of the film diameter. All the assessments were performed on the Raith eLiNE system operating in SEM mode at 20 kV.

Cutting the Gold Particle with Focused Ion Beam. Gold particles that appeared to possess openings atop the particles as observed using the Raith eLiNE SEM, were randomly selected as candidates for cross-section cutting by focused ion beam milling. A FEI FIB 200 XP focused ion beam system, using a gallium ion beam that operates at 30 kV (50 k × magnification, 1 pA current, and 10 nm resolution), was used to cross-section the hollow particle. The gold particles were cut from the edge to the center using the focused gallium beam with the same acceleration voltage (30 kV) and constant beam current (1pA), but employing different drilling time per slice. Thus, the cutting depth depended on the actual shape of the particle. Known as the cleaning cross-section tool, this instrument can minimize the redeposition from the substrate. Once the particles were dissected in half by the focused gallium beam, the samples were immediately transferred to a Hitachi S4200 SEM for imaging; this allowed us to minimize the damage and reposition caused by the gallium source in FIB, when the FEI system was used in imaging mode. This procedure allowed us to examine the topology and morphology of the cross-sectioned region.

Optical Response and near Field Enhancement Investigation Using PEEM. To investigate the plasmonic near field enhancement, PEEM was employed to image the photoexcited electrons from the solid and hollow gold particles. After synthesis, the samples were transferred to the UHV PEEM chamber and exposed to a 150 fs pulsed laser centered at 400 nm at an incident angle of 15°

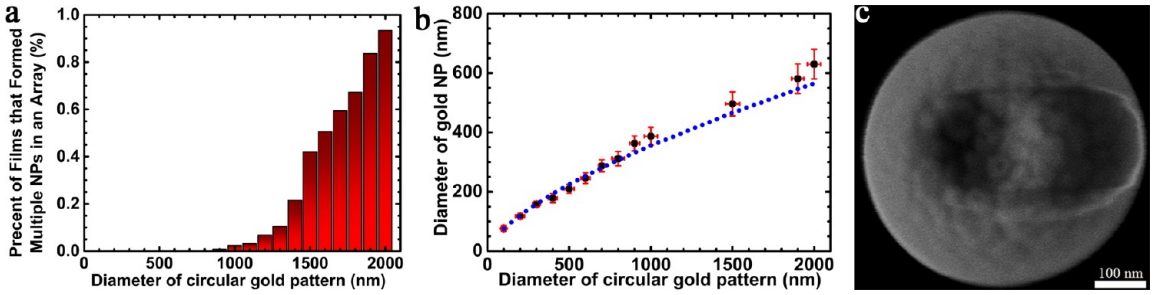

Figure 2. (a) Graph representing the percent of gold films that form multiple particles (multiple-particle films) as a function of the film diameter. Each array with different diameter contained 50 × 50 annealed samples. The onset diameter of the multiple-particle films was 900 nm. (b) A graph of the resulting particle diameter as a function of the gold patterned film diameter. Note that only single particle formation from one film is counted. The uncertainty in the particle diameter comprises the standard deviation in the particle diameter of all particles formed from a single film of a single diameter. The dotted line is a theoretical calculation of the as-formed, solid particle diameter as a function of patterned film diameter, based on an equivalent volume match analysis. (c) SEM image of a hollow gold particle of diameter approximately 500 nm, formed solely from a gold film of diameter of 2000 nm. The top opening along the surface of the particle affirmed its hollow morphology.

with respect to the sample surface. The PEEM imaging system, used in this study, is described in detail elsewhere.[13]

RESULT AND DISCUSSION

After annealing, all patterned film of a diameter less than 900 nm consistently yielded a single particle, as evidenced in Figure 1b. For each array, the resulting gold particles maintained good size uniformity. The particles did not migrate across the substrate, remaining at the same location where the patterned films were originally deposited. The interpattern spacing was large enough to suppress coarsening among neighboring films.[14] Notably, when the diameter of patterned film increased to 900 nm, the average number of gold particles formed at each film began to increase. In other words, they apparently began to divide into multiple particles after the annealing step, as evidenced in Figure 1c. Although multiple-particle films (films that yielded multiple particles) accounted for a very small percent of the observed yield at the 900 nm diameter, this diameter appeared to have defined the critical diameter of film at which multiple gold particles formed.

As expected, when the film diameter increased above 900 nm, the number of films that yielded multiple-particles gradually increased. In this regime, beyond the uncertainty in the patterned-film diameter (±20 nm), a finite probability existed for the patterned film to coalesce either into a single large particle or split to smaller particles; this probability depended on the initial diameter of the patterned film, as discussed later. The two distinct behaviors of the patterned film may be due to the local variations in the external conditions, such as the substrate roughness and the flow rate of nitrogen during the particle fabrication. An example of this can be seen in Figure 1d, for which arrays of gold particles were formed from patterned-films of diameter = 2000 nm. Both single and multiple gold particles were observed and obviously the multiple particles accounted for the majority. Interestingly, a large fraction of the single large gold particles were observed to be hollow, as shown in the inset of Figure 1d. A histogram of the relationship between the diameter of the initial patterned-film and the percentage of multiple-particle film, defined by the ratio between patterned-films that yielded multiple particles and the amount of patterned-films in an array (the amount were set to be the same for all sizes), is provided in Figure 2a. This histogram indicates the onset diameter of the multiple-particle film. The percentage of multiple-particle film increased nonlinearly as the diameter grew above the onset diameter. For the largest film (2000 nm), only a small fraction (<10%) formed a single large particle. After prolonged annealing periods for the films (periods >20 h), no agglomeration of smaller particles into large clusters of particles or into larger individual particles was seen.

The relationship between the diameter of the patterned film and the diameter of the resultant gold particles is shown in Figure 2b; for this graph, only patterned-films that produced single particle were assessed. For those films with diameters less than 900 nm (onset diameter), the diameters of the resultant particles exhibited a clear linear relationship (presuming the particles were solid objects), including relatively small polydispersity. These results confirmed that the diameters of the particles were easily tuned as a function of the film size. The smallest particles in our study have a diameter of approximately 70 nm, fabricated via annealing a 100 nm-patterned-film, as shown in Supporting Information, Figure S1. The size of the resulting particles can be produced in even smaller diameters by annealing a smaller and thinner patterned-film.

Our patterned film experiment also confirmed the observation of hollow gold particles, fabricated through the same annealing process. Annealing large gold films (diameter ≥900 nm) resulted in two types of particle arrays: (1) multiple small gold particles; and (2) one single large gold particle. Analysis of SEM images suggests that the vast majority of small gold particle clusters (diameter < 300 nm) formed from large film (diameter ≥ 900) appeared to be solid; no distinguishable hollow surface character is observed. However, for some of the larger gold particles (diameter >400 nm), hollow structures were attained, which may be an equilibrium condition for the deposited film thickness since annealing thinner gold film yielded much smaller particles (details in Supporting Information, Figure S2). Based on our assessment of the SEM images, the percentage of hollow gold particles that were formed is ∼70% in the samples that were fabricated from the 20 nm thick Au films, as observed in Figure 1d. An image of such a structure, detailing the surface topography of the hollow gold particle, is provided in Figure 2c (Also see Figure 1d). The openings of the hollow cage-like structures were readily apparent under SEM; the interior contours were evident, which affirmed their hollow conformation. To interrogate the particles further, we removed the particles from their underlying substrate and dropcast them onto a ransmission electron microscopy (TEM) grid for analysis (Philips CM 200 at 200 kV). The TEM images, shown in Supporting

Information, Figure S3, indicated that the particles were composed of a thick gold shell with a rough, textured surface.

Moreover, we found that some instances of the multiple-particle film also yielded hollow particles, as long as the diameters of the as-formed gold particles were larger than 400 nm. Evidence of this is provided in Figure 3. In this example,

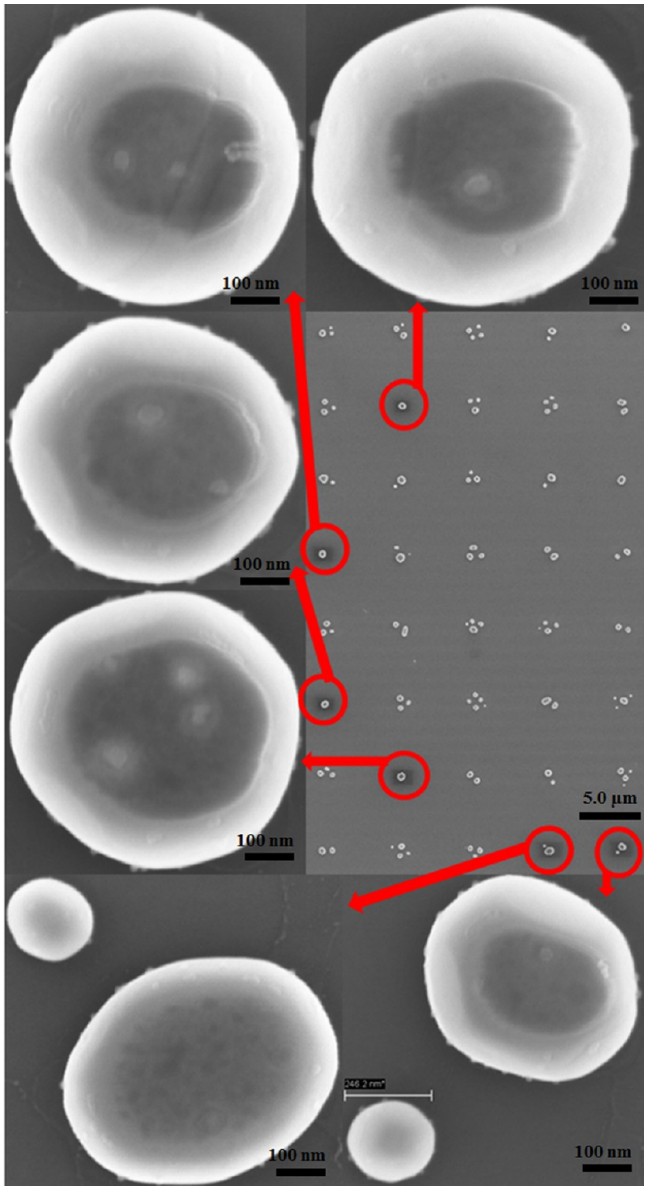

Figure 3. SEM images of several single large hollow particles formed from gold films array with diameter of 2000 nm.

the diameter of the patterned film was 2000 nm. The particles, highlighted by red circles in the figure, have diameters that were larger than 400 nm. Each of the particles notably possessed hollow structure, including those that comprised part of a multiple particle configuration (note the bottom two images of Figure 3 and the inset of Figure 1d). All other samples (film diameter =1500−1900 nm) possessed the same feature as this example.

To validate the observation further, a theoretical calculation to volume match for the diameter of the as-formed solid particle as a function of the patterned film diameter was considered, based on the equation:

$$\pi\left(\frac{d_1}{2}\right)^2 h_0 = \frac{4}{3}\pi\left(\frac{d_2}{2}\right)^3 \times \frac{2}{3} \quad (1)$$

where d_1 is the diameter of the circular, cylindrical gold film, d_2 is the diameter of the resulting particle, and h_0 is the thickness of the film ($h_0 = 20 \pm 2$ nm). The factor of 2/3 accounts for the actual shape of our dome-like particles. The relationship between d_1 and d_2 was plotted as a dotted curve in Figure 2b. For film diameters ≤900 nm (corresponding to the as-formed solid particles with diameter ≤400 nm), all experimental data fall onto the fit curve, implying the formation of solid particles. In contrast for diameters >900 nm, the experimental data start to deviate from the fit curve, which meant that the particle diameter grew bigger than what would be expected for a solid particle. Such a phenomenon could be attributed to a hollow nanostructure for the particles. For the datum point for the film diameter of 2000 nm (corresponding to an average diameter of the as-formed 600 nm particles), despite the large error bar, its minimum value was still noticeably larger than the expected solid value, which was strong evidence of the appearance of the hollow particles. This juxtaposition of our particle data and the volume match calculation confirmed that only hollow particles formed in the region of large film diameter (>900 nm) and with a large resulting particle diameter (>400 nm), consistent with our observation in Figure 3. Thus, we concluded that sufficiently large gold films (larger than a critical diameter), with a significantly high probability, yield hollow-structured particles.

To complement our SEM analysis of the hollow, intact particles and to illustrate more effectively the geometry of the nanovoid inside the gold hollow nanostructure, a tilted (45°) SEM image of a particle cross-section was acquired, as shown in Figure 4. Figure 4a shows the cross-section of a randomly selected gold particle with diameter of 500 nm, which formed solely from a 2000 nm patterned film. This particle possesses obvious openings viewed in the normal mode in SEM. The morphology of the nanovoid as well as the geometry shape of the particle may be different from that observed from nontilted SEM because of the surface redeposition induced by high energy FIB cutting. However, the strong contrast between the edge and the center evinces the existence of the nanovoid, composed of a shell of thickness ∼100 nm; this is consistent with the results acquired by TEM (Supporting Information, Figure. S4). Similar results are obtained in other large particles. For comparison, a cross-section of a solid particle with smaller size (diameter of ∼300 nm) is presented in Figure 4b; the particle in this image exhibits a smooth surface morphology without any contrast change, indicative of a solid particle.

To compare the near-field, plasmonic enhancement of the solid and hollow gold particles, two samples were chosen for analysis: (1) single solid gold particles, prepared from 20 nm thick circular gold patterns, of a diameter of 900 nm; and (2) multiple gold particles composed of both smaller solid gold particles and larger hollow particles, prepared from 20 nm thick circular gold patterns, of a diameter of 2000 nm. The results, from excitation with a 400 nm, 150 fs pulsed laser (Figures 5a and 5b), and a UV mercury arc lamp (Figure 5c), are shown in Figure 5. The mercury arc lamp was predominantly used for imaging the sample surface and provided a linear photo-emission response (single-photon process) from both the flat SiO_2 surface and the gold particles. When we illuminated the sample using the laser, regions that contained both the solid and hollow particles were significantly brighter than the

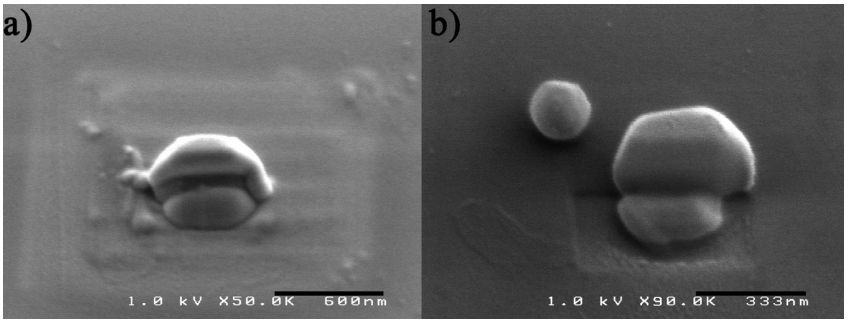

Figure 4. (a) Tilted (45°) SEM image of the cross-section of a gold hollow particle after preparation by FIB, which eliminated half of the particle from the center. The interior void is clearly observed through the strong contrast between the edge of the shell of the particle and the center of the particle. (b) Tilted SEM image of the cross-sectioned region of a solid gold particle, presented in juxtaposition with panel a.

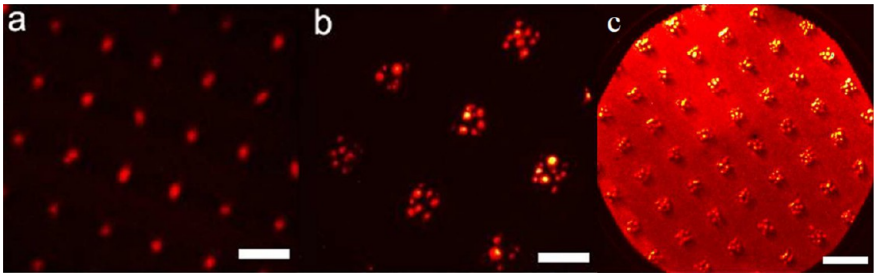

Figure 5. PEEM images of (a) the solid Au particles and (b) multiple gold particles containing both smaller solid gold particles and larger hollow particles. Both images were acquired using a 400 nm femtosecond laser. The associated field-of-view for these images was 30 μm. Scale bar = 3 μm. (c) PEEM image of the surface of the same sample as described in (b), taken with a mercury arc lamp. Scale bar = 5 μm.

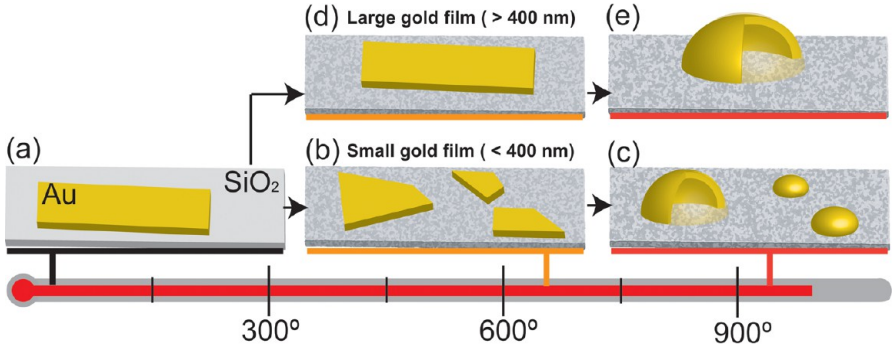

Figure 6. Illustration of the formation mechanism of the gold particles on SiO_2/Si.

surrounding flat SiO_2 surface. This was because the resonant localized surface plasmon (LSP) modes of the gold particles coupled with the incoming electric field (due to laser), leading to an enhancement of the field intensity in the vicinity of the particles. Since the laser energy, 3.1 eV (400 nm), is below the work function of gold (>5.0 eV), the enhanced field intensity over the gold particles was most probably due to the nonlinear (two-photon) photoemission from the particles upon laser illumination.[15,16] Interestingly, the larger gold particles exhibited a greater plasmonic field enhancement when compared with the smaller particles. This behavior was attributed to the hollow nature of the larger particles, which is expected to facilitate the nonlinear photoemission of gold metal under laser illumination;[17,18] such a response also supports our analysis that the percentage of hollow particles was ~70%. This greater enhancement observed from the hollow gold particles makes them attractive candidates for photoelectric and sensing applications.

A schematic of the formation mechanism of the gold particles originating from a gold film is shown in Figure 6. The growth of our gold particle from flat films can be attributed to the different wettabilities of the gold (hydrophobic) and the underlying SiO_2 substrate (hydrophilic). A native silicon dioxide layer (~2 nm) formed atop our silicon substrate prior to the gold deposition. Its presence was confirmed by ellipsometry measurements. The melting of the SiO_2 was observed at ~650 °C. Coupled with the large, weakly temperature-dependent contact angle between gold and SiO_2 (θ ~140°), we concluded that three-dimensional, spherical gold nanostructures are thermodynamically preferred to form on SiO_2 over planar structures.[19] Although the interfacial coupling between gold and SiO_2 is rather weak, a certain temperature (thermal energy) is still needed to overcome the activation barrier of the reconstruction, that is, to break the interfacial coupling between the surfaces. We used a uniform gold film to simulate the thermal behavior of large gold patterned films in our study. Temperature-controlled and time-controlled experi-

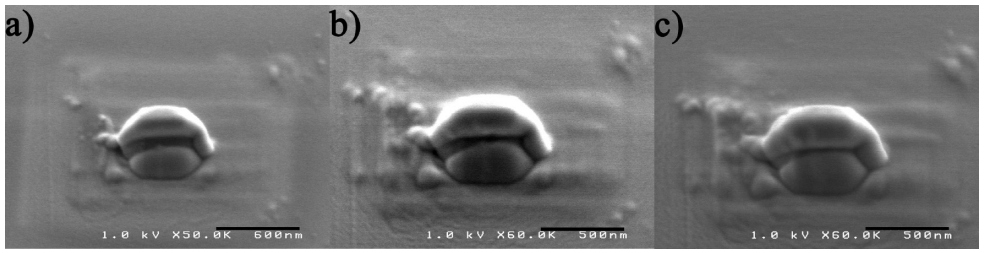

Figure 7. Time evolved, tilted (45°) SEM images of a half-cutting gold hollow particle upon electron beam heating. (a) At 0 h of SEM imaging. (b) After 0.5 h of imaging. (c) After 1.0 h of imaging. The void inside the particle was observed to collapse gradually.

ments were performed, the results of which are shown in Supporting Information, Figures S4 and S5; these confirmed the melt of SiO_2 and the aforementioned proposed mechanism.

Further, we try to explain the size dependence of the splitting of the patterned film at some onset boundary under certain thermal conditions. Spinodal decomposition (also known as thermal dewetting) during the heating and coarsening during the cooling account for the formation of multiple particles from large films.[11,14,20−22] Grain boundary grooving may also contribute to the rupture of the thin film since they are poly crystalline. A thermal model that describes the spontaneous rupture of a thin film was considered.[22] When the gold films were annealed at an elevated temperature (~940 °C), thermal fluctuations, due to varying interface interactions between the gold and the underlying substrate, likely induced perturbative oscillations across the film that led to deformations of the film from its original structure and morphology. The magnitude of the perturbation is characterized by the critical wavelength, λ_c:[23]

$$\lambda_c = {h_0}^2 \sqrt{\frac{4\pi^3\sigma}{A}} \tag{2}$$

where σ is the temperature-dependent surface tension of the film material, A is the Hamaker constant of the film material on the specific underlying substrate, and h_0 is the thickness of the film. This thermal model is intuitively consistent with our experimental observation: as the thickness of the film decreases, the onset boundary of multiple particle formation tends to be smaller, that is, the perturbation wavelength shortens and becomes more effective for smaller films. Therefore, films of a diameter smaller than the critical wavelength tend to be stable. In other words, they have very little probability to deform under ambient thermal conditions.

As the diameter of the film exceeds λ_c, the deformation probability of the patterned film increases (Figure 6b), which is consistent with the histogram in Figure 2a. The film breaks into irregularly shaped gold flakes, which tend to curve to minimize the surface energy and sequentially turn into multiple gold particles on the SiO_2 substrate (Figure 6c). Additionally, large gold particles have a low probability to form without cracking the original gold film into smaller pieces (Figures 6d and 6e). Experimental values from the literature for these variables to approximate λ_c for our conditions (σ = 0.27 N/m,[24−26] A = 410 zJ,[27,28] and h_0 = 20 ± 5 nm) yielded a lower limit of 2.0 μm, which is comparable to the onset diameter that we observed for the production of multiple particles.[24−30] If the substrate defects are incorporated, it would enhance the rupture probability for the gold film. Even though the calculated λ_c is of the same order-of-magnitude as our experimentally determined onset diameter (900 nm), this result suggests that the effective Hamaker constant for our nanoscale gold films atop SiO_2 in a nitrogen environment and/or the effective surface tension of our films could be substantially different (for example, larger for A and smaller for σ) from what others have measured for similar metallic thin films. Experimental measurement of the temperature-dependence of the Hamaker constant and the surface tension of our nanostructures will provide key information to refine the hollow/solid particle production ratio and to scale-up the overall particle fabrication quantity.

Size-dependent thermal stability may account for the formation of the large hollow gold particles observed in our experiments. The various sizes of the particles resulted in different surface tension and surface free energy, which dominated their thermal stability.[31−33] Since the high annealing temperature used in our study, most of the ruptured gold flakes underwent a nonequilibrium thermal process, which may have produced a nanovoid inside of the structure when the flat film was reconstructed into spherical particles. Since the small particles maintained a larger surface-to-volume ratio, they were more likely to recrystallize, forming solid spheres at a relatively lower temperature (<940 °C) compared to the larger ones. This mechanism explains why hollow structures were only observed for large gold particles (Figure 2c) with a threshold diameter (as-formed particles diameter of 400 nm). To verify the instability of the hollow particle, we examined the FIB-cut, hollow particle in SEM over an extended period of time. Figure 7 shows images of the time evolution of the FIB-cut, hollow particle. The exposed nanovoid was gradually infiltrated by electron beam-assisted redeposition of carbon, extant in the SEM chamber, and surface reconstruction of the gold that composed the particle.[34] This assessment demonstrated the relative instability of the hollow nanostructures, exposed to low-energy electron radiation.

■ CONCLUSION

In summary, we proposed a promising technique for the fabrication of gold particles with tunable size and hollow structure. A critical size for the diameter of the gold patterned film was identified, below which the formation of single particles dominate and above which the formation of multiple particles occurred. Hollow gold particles were also fabricated from lithographically patterned films of sufficiently large diameter. Possible mechanisms for the growth of these particles were explored. Combined with the characterization of the near field enhancement of the hollow structures, this study provides a new avenue for the production of metallic nanostructures which could have broad employment in plasmonics, sensing devices, and other applications.

■ ASSOCIATED CONTENT

Supporting Information

Additional information regarding time-controlled and temperature-controlled synthesis experiments, and additional TEM images of the gold particles. This material is available free of charge via the Internet at http://pubs.acs.org.

■ AUTHOR INFORMATION

Corresponding Author

*E-mail: james.h.dickerson@vanderbilt.edu.

Author Contributions

#These authors contributed equally to this work.

Notes

The authors declare no competing financial interest.

■ ACKNOWLEDGMENTS

This research is partially supported by the National Science Foundation (NSF): Awards DMR-0757380 and CAREER DMR-1054161 (J.L., W.H., M.R., and J.H.D.), DTRA Grant No. HDTRA1-10-1-0047 (B.W. and S.T.P.), Center for Science Outreach at Vanderbilt University (S.P.), and the William A. and Nancy F. McMinn Endowment (S.T.P.). Portions of this work were performed at the Vanderbilt Institute of Nanoscale Science and Engineering, using facilities renovated under NSF ARI-R2 DMR-0963361.

■ REFERENCES

(1) Sánchez-Iglesias, A.; Pastoriza-Santos, I.; Pérez-Juste, J.; Rodríguez-González, B.; García de Abajo, F. J.; Liz-Marzán, L. M. *Adv. Mater.* **2006**, *18* (19), 2529−2534.

(2) Wheeler, D. A.; Newhouse, R. J.; Wang, H. N.; Zou, S. L.; Zhang, J. Z. *J. Phys. Chem. C* **2010**, *114* (42), 18126−18133.

(3) Dowgiallo, A.-M.; Schwartzberg, A. M.; Knappenberger, K. L., Jr. *Nano Lett.* **2011**, *11* (8), 3258−3262.

(4) Chandra, M.; Dowgiallo, A.-M.; Knappenberger, K. L., Jr. *J. Am. Chem. Soc.* **2010**, *132* (44), 15782−15789.

(5) Mahmoud, M. A.; El-Sayed, M. A. *J. Am. Chem. Soc.* **2010**, *132* (36), 12704−12710.

(6) Mahmoud, M. A.; Snyder, B.; El-Sayed, M. A. *J. Phys. Chem. C* **2010**, *114* (16), 7436−7443.

(7) Xie, H.-n.; Larmour, I. A.; Smith, W. E.; Faulds, K.; Graham, D. *J. Phys. Chem. C* **2012**, *116* (14), 8338−8342.

(8) Brolo, A. G.; Gordon, R.; Leathem, B.; Kavanagh, K. L. *Langmuir* **2004**, *20* (12), 4813−4815.

(9) Righini, M.; Zelenina, A. S.; Girard, C.; Quidant, R. *Nat. Phys.* **2007**, *3* (7), 477.

(10) Bechelany, M.; Maeder, X.; Riesterer, J.; Hankache, J.; Lerose, D.; Christiansen, S.; Michler, J.; Philippe, L. *Cryst. Growth Des.* **2010**, *10* (2), 587−596.

(11) Tan, B. J. Y.; Sow, C. H.; Koh, T. S.; Chin, K. C.; Wee, A. T. S.; Ong, C. K. *J. Phys. Chem. B* **2005**, *109* (22), 11100−11109.

(12) Mueller, C. M.; Mornaghini, F. C. F.; Spolenak, R. *Nanotechnology* **2008**, *19* (48), 485306.

(13) Peppernick, S. J.; Joly, A. G.; Beck, K. M.; Hess, W. P. *J. Chem. Phys.* **2011**, *134* (3), 034507.

(14) Blunt, M. O.; Martin, C. P.; Ahola Tuomi, M.; Pauliac Vaujour, E.; Sharp, P.; Nativo, P.; Brust, M.; Moriarty, P. J. *Nat. Nanotechnol.* **2007**, *2* (3), 167−170.

(15) Xiong, G.; Shao, R.; Droubay, T. C.; Joly, A. G.; Beck, K. M.; Chambers, S. A.; Hess, W. P. *Adv. Funct. Mater.* **2007**, *17* (13), 2133−2138.

(16) He, W.; Vilayurganapathy, S.; Joly, A. G.; Droubay, T. C.; Chambers, S. A.; Maldonado, J. R.; Hess, W. P. *Appl. Phys. Lett.* **2013**, *102* (7), 071604.

(17) Polyakov, A.; Senft, C.; Thompson, K. F.; Feng, J.; Cabrini, S.; Schuck, P. J.; Padmore, H. A.; Peppernick, S. J.; Hess, W. P. *Phys. Rev. Lett.* **2013**, *110* (7), 076802.

(18) El-Khoury, P. Z.; Hu, D.; Apkarian, V. A.; Hess, W. P. *Nano Lett.* **2013**, *13* (4), 1858−1861.

(19) Cahn, R. W.; Eustathopoulus, N.; Nicolas, M. G.; Drevet, B. Wettability at High Temperatures. In *Pergamon Materials Series*; Eustathopoulus, N., Nicolas, M. G., Drevet, B., Eds.; Pergamon: Cambridge, U.K., 1999; Vol. 3, p xi.

(20) Cahn, J. W. *Acta Metall.* **1961**, *9* (9), 795−801.

(21) Cahn, J. W. *Acta Metall.* **1966**, *14* (12), 1685−1692.

(22) Huston, E. L.; Cahn, J. W.; Hilliard, J. E. *Acta Metall.* **1966**, *14* (9), 1053−1062.

(23) Ruckenstein, E.; Jain, R. K. *J. Chem. Soc., Faraday Trans. II* **1974**, *70*, 132−147.

(24) Chushak, Y. G.; Bartell, L. S. *J. Phys. Chem. B* **2001**, *105* (47), 11605−11614.

(25) Nanda, K. K.; Sahu, S. N.; Behera, S. N. *Phys. Rev. A* **2002**, *66* (1), 8.

(26) Sambles, J. R. *Proc. R. Soc. A* **1971**, *324* (1558), 339−351.

(27) Butt, H. J.; Cappella, B.; Kappl, M. *Surf. Sci. Rep.* **2005**, *59* (1−6), 1−152.

(28) Ye, Y.; Yuan, X.; Xiang, X.; Dai, W.; Chen, M.; Miao, X.; Lv, H.; Wang, H.; Zheng, W. *Opt. Lasers Eng.* **2011**, *49* (4), 536−541.

(29) Colton, R. J.; Barger, W. R.; Baselt, D. R.; Corcoran, S. G.; Koleske, D. D.; Lee, G. U., *Atomic force microscopy: Surface forces, adhesion, and nanomechanics measurements*. VSP Publishers: Utrecht, 1998; Vol. *1*, p 900.

(30) Egry, I.; Lohoefer, G.; Jacobs, G. *Phys. Rev. Lett.* **1995**, *75* (22), 4043−4046.

(31) Dick, K.; Dhanasekaran, T.; Zhang, Z.; Meisel, D. *J. Am. Chem. Soc.* **2002**, *124* (10), 2312−2317.

(32) Koga, K.; Ikeshoji, T.; Sugawara, K.-i. *Phys. Rev. Lett.* **2004**, *92* (11), 115507.

(33) Wang, N.; Rokhlin, S. I.; Farson, D. F. *Nanotechnology* **2008**, *19* (41), 415701.

(34) Rykaczewski, K.; Scott, J. H. J.; Fedorov, A. G. *Appl. Phys. Lett.* **2011**, *98* (9), 093106.